Sains Malaysiana 48(2)(2019): 369–375
http://dx.doi.org/10.17576/jsm-2019-4802-14

Growth and Magnetic Behaviours of $La_{0.7}Sr_{0.3}MnO_3$ Nanoparticles Synthesized via Thermal Treatment Method

(Tingkah Laku Pertumbuhan dan Magnetik Nanopartikel $La_{0.7}Sr_{0.3}MnO_3$ Disintesis melalui Kaedah Rawatan Terma)

PAN KAI YAP, ABDUL HALIM SHAARI*, HUSSEIN BAQIAH, CHEN SOO KIEN, JUMIAH HASSAN, MOHD MUSTAFA AWANG KECHIK, LIM KEAN PAH & ZAINAL ABIDIN TALIB

ABSTRACT

$La_{0.7}Sr_{0.3}MnO_3$ (LSMO) nanoparticles were synthesized by thermal treatment method using water as solvent and polyvinyl pyrollidone (PVP) as capping agent. The as prepared precursor was calcined at various temperatures ranging from 500°C to 1000°C. Structural characterization using X-rays diffractions (XRD) showed that the LSMO nanoparticles, calcined at temperature ≥ 600°C, have single phase of $La_{0.7}Sr_{0.3}MnO_3$ with rhombohedral crystal structure without any secondary phases being detected. The average particle size of nanoparticles increased gradually from 23 to 163 nm for samples calcined at 500 to 1000°C. Magnetic measurement at room temperature using vibrating sample magnetometer (VSM) indicated that the LSMO nanoparticles had soft ferromagnetic behaviour with coercivity ranged from 3.43 to 33.78 G. The magnetic saturation (M_s) of nanoparticles increased with the increment of particle size. From Electron Spin Resonance (ESR) measurement, the g-value of LSMO nanoparticles increased with the increasing of calcination temperature. The ESR indicated a coexistence of ferromagnetic and paramagnetic phases in LSMO nanoparticles below Curie temperature (T_c). The T_c was in the range of 50-80°C for LSMO calcined at 500°C and it is in the range of 80-110°C for LSMO calcined 600, 700, 800, 900, and 1000°C.

Keywords: Electron resonance; magnetic properties; nanostructures; Rietveld analysis; thermal treatment

ABSTRAK

Zarah nano $La_{0.7}Sr_{0.3}MnO_3$ (LSMO) telah disintesis melalui kaedah rawatan terma menggunakan air sebagai pelarut dan polivinil pirolidon (PVP) sebagai agen penyalutan. Prekursor yang disediakan telah melalui pengkalsinan pada suhu yang berbeza dari 500°C hingga 1000°C. Pencirian struktur menggunakan pembelauan sinar-X (XRD) mendedahkan bahawa zarah nano LSMO, dikalsinkan pada suhu ≥600°C, mempunyai struktur fasa tunggal tanpa sebarang fasa sekunder yang dikesan. Purata saiz zarah bagi zarah nano meningkat secara beransur-ansur daripada 23 hingga 163 nm untuk sampel yang dikalsin pada suhu 500 hingga 1000°C. Pengukuran sifat magnet pada suhu bilik menggunakan magnetometer sampel bergetar (VSM) menunjukkan bahawa zarah nano LSMO mempunyai kelakuan feromagnet lembut dengan koersiviti berjulat antara 3.43 hingga 33.78 G. Ketepuan magnet (M_s) zarah nano meningkat dengan kenaikan saiz zarah. Daripada pengukuran resonans spin elektron (ESR), nilai g bagi zarah nano LSMO meningkat dengan peningkatan suhu kelembapan pengkalsinan. ESR juga menunjukkan kewujudan bersama fasa feromagnet dan paramagnet dalam zarah nano LSMO di bawah suhu Curie (Tc). Tc berada dalam lingkungan antara 50-80°C untuk LSMO yang dikalsin pada suhu 500°C dan ia berada dalam lingkungan antara 80-110°C untuk LSMO yang dikalsinkan pada suhu 600, 700, 800, 900 dan 1000°C.

Kata kunci: Analisis Rietveld; nanostruktur; rawatan terma; resonans elektron; sifat magnetik

INTRODUCTION

Perovskite manganites $La_{1-x}A_xMnO_3$ (A = Ca, Sr, Ba) have attracted much attention since the discovery of intrinsic and extrinsic colossal magnetoresistance (CMR) effect in 1990s (Hwang et al. 1996). The intrinsic CMR occurred in the vicinity of the ferromagnetic metallic state to paramagnetic insulator state as the temperature increases, under several values of magnetic fields (Hwang et al. 1996; Urushibara et al. 1995). The correlation between magnetic and electrical properties of manganites had been well explained by double exchange theory (Zener 1951) and Jahn-Teller distortion (Millis 1995). On the other hand, the extrinsic CMR effect occurred in polycrystalline manganites, is due to the spin polarized tunneling between the grain boundaries (Gupta & Sun 1999). This enormous characteristic is useful for technology application such as magnetic data storage and magnetic sensors (Lopez-Quintela et al. 2003).

Lots of fundamental studies have been carried out by tailoring the elements and composition of *A* for the understanding of the magnetic, electrical and structural behaviours of manganites families. $La_{0.7}Sr_{0.3}MnO_3$ (LSMO) is one of the most attractive compound due to its high Curie temperature (T_c ~ 370 K) and excellent in magnetic, electrical properties (Daengsakul et al. 2009a; Rajagopal et al. 2006). Recently, some of the findings are concentrated on the nanoscale of manganites (Andrade et

al. 2016; Moradi et al. 2014). It is found that the magnetic and electrical properties of manganites are dependent on their size (Dyakonov et al. 2010). Nanoparticles of manganites may exist in single magnetic domain and have magnetic disorder at the surface. These two characteristics are associated with different physical properties than the micron size manganites (Dutta 2003). Recently, some researchers have found that the single domain LSMO nanoparticles exhibits superparamagnetism behaviour below a critical size. This phenomena has high potential in biomedical applications (Daengsakul et al. 2009a, 2009b; Thorat et al. 2012).

Many methods have been made to produce manganites in nanoscale including sol-gel (Ehi-Eromosele et al. 2016; Karthikeyan 2014; Pan et al. 2012), co-precipitation (Drofenik 2007; Ghosh et al. 2005) and hydrothermal techniques (Lee et al. 2006; Teng 2009). However, these methods have complicated procedure such as control of pH and materials concentrations and may use toxic reagent such as ethylene glycol, oxalic acid or ammonia hydroxide, which may potentially harm the environment with the by-products after reaction (Naseri et al. 2011a). Moreover, the final product of LSMO phase may be associated with other secondary phases such as $SrMnO_3$ (Ehi-Eromosele et al. 2016). In this work, we have employed thermal treatment methods to prepare LSMO nanoparticles at different temperature (500-1000°C) using aqueous solution of metals nitrates and capping agent of polyvinyl pyrollidone (PVP) without addition of other chemicals. This method is advantageous because it is simple, low cost, and environment friendly (Naseri et al. 2011b). The LSMO nanoparticles calcined at temperature ≥ 600°C have single phase structure without any secondary phases being detected. The magnetic behaviours of LSMO nanoparticles were investigated using vibrating sample magnetometer (VSM) and electron spin resonance (ESR).

Materials and Methods

The synthesis of $La_{0.7}Sr_{0.3}MnO_3$ (LSMO) nanoparticles was based on thermal treatments aqueous solution of metals nitrates and polyvinyl pyrrolidone (PVP) that acts as a capping agent. First, a 4 wt. % of polyvinyl pyrrolidone (PVP, MW = 10,000) was dissolved in deionized water at 70°C before mixing with the stoichiometry amount of metal nitrates, i.e. $La(NO_3)_3.6H_2O$, $Mn(NO_3)_2.4H_2O$ and $Sr(NO_3)_2$ under hot plate at 80°C and stirred for 2 h. A transparent yellowish solution was obtained without any observation of precipitation. The solution was heated in an oven at 80°C until a formation of dry yellowish solid remains. The solid was further crushed into fine powder and heated for 10 h at various calcination temperatures (*C.T.*) ranging of 500, 600, 700, 800, 900, and 1000°C, respectively.

Thermal decomposition of LSMO precursor was evaluated by Thermogravimetric Analysis (TGA, Mettler Toledo TGA/SDTA851e) with the heating rate of 10°C/min from 50°C up to 1000°C. The structural behaviours of the LSMO nanopowders were characterized by X-ray diffractometer (XRD; PHILIPS PW 3040) using Cu Kα radiation at room temperature. Rietveld analysis was performed using X'Pert HighScore Plus software. Morphological studies were done by using Field Emission Scanning Electron Microscope (FESEM, JSM-7600F). The magnetic properties of all samples were determined by using vibrating sample magnetometer (VSM, Lakeshore 7400) at room temperature with the field up to 10 kG and X-band Spectrometer (JEOL, Tokyo) for Electron Spin Resonance (ESR) Signal measurement at room and certain temperatures above room temperature in the magnetic field of 0 - 600 mT with microwave frequency, f = 9.195 GHz.

Results and Discussion

Thermogravimetric Analysis (TGA) curve of as-prepared LSMO precursor is shown in Figure 1. From the curve, the weight loss of the precursor can be divided into three different regions through the increasing of temperature. The first weight loss region in between ~ 56 to ~ 175°C is attributed to the dissociative and coordinated water molecules. The second region, which is in between ~ 243 and ~ 335°C, experienced in decomposition of nitrates organic components. The decomposition of PVP occurred in the third region, within the temperature range of ~ 337 to ~ 553°C (Du et al. 2006). All the organic compounds were eliminated successfully after the third region weight loss. Weight loss after the third region (> 600°C) confirmed the formation of stable pure LSMO perovskite structure.

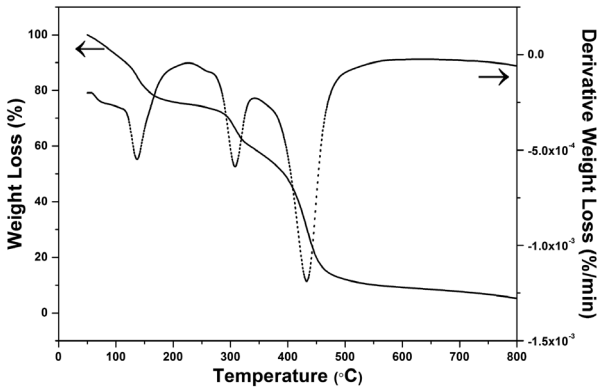

FIGURE 1. TGA curve of LSMO as prepared precursor

Room temperature XRD patterns of LSMO nanopowders with different calcination temperature are shown in Figure 2(A). The low intensity and broad peaks of the as-prepared precursor imply the domination of amorphous phase structure. Sample calcined at 500°C has sharp diffraction peaks indicating the formation of metal oxide. However, pure perovskite structure is only formed when the calcination temperature is adjusted to 600°C and above. No secondary phase is detected from for samples calcined at *C. T.* = 600 – 1000. The diffraction peaks of these calcined samples can be fitted using Rietveld method into ICSD standards (ICSD Reference Code: 98-

010-9891), where rhombohedral structure is formed with space group *R-3c*. Figure 2(B) displays the observed and calculated XRD patterns after refinement for the sample calcined at 1000ºC. The estimated lattice parameters of the previous sample 1000ºC were $a = b = 5.504$ Å and $c = 13.366$ Å. Average crystallite size of LSMO nanoparticles was calculated by measuring the full-width half-maxima (FWHM) of the highest intensity peak ($2\theta \sim 32° - 33°$) by using the Scherrer's formula, the data is displayed in Table 1. It is clearly seen that the average crystallite size of LSMO samples increases with the increasing of calcination temperature.

Surface morphologies of prepared LSMO samples were studied by FESEM and the micrographs is presented in Figure 3. The sizes of nanoparticles increased with the increasing of calcination temperature. The increase of calcination temperature leads to particle grain growth due to diffusion; hence enhancing the overall particle size. The average particle size of each samples was calculated from 100 grains taken from the micrographs. The calculated particle sizes are ~ 23, 29, 37, 47, 67 and 163 nm for samples calcined at 500, 600, 700, 800, 900, and 1000ºC, respectively.

The room temperature magnetic properties of LSMO nanoparticles were determined by magnetization ($M - H$) curve with the field up to 10 kG, as displays in Figure 4. All the LSMO samples showed soft ferromagnetic ordering behaviour with the shape of sigmoid function. The magnetization saturation (M_s) at 10 kG field is obtained and shown in Table 1. The ascending of magnetization value

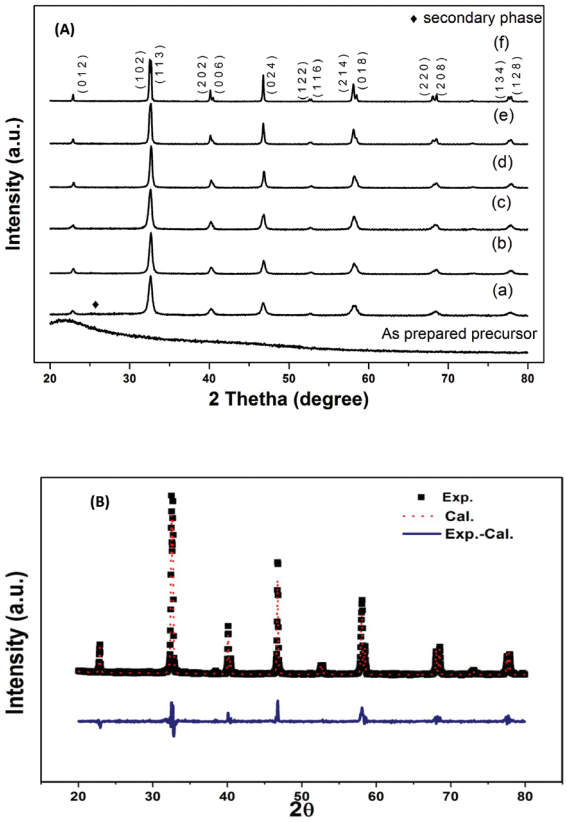

FIGURE 2. (A) XRD patterns of LSMO as-prepared precursor and calcined at (a) 500, (b) 600, (c) 700, (d) 800, (e) 900, and (f) 1000ºC. (B). Rietveld analysis of XRD patterns of sample calcined at 1000

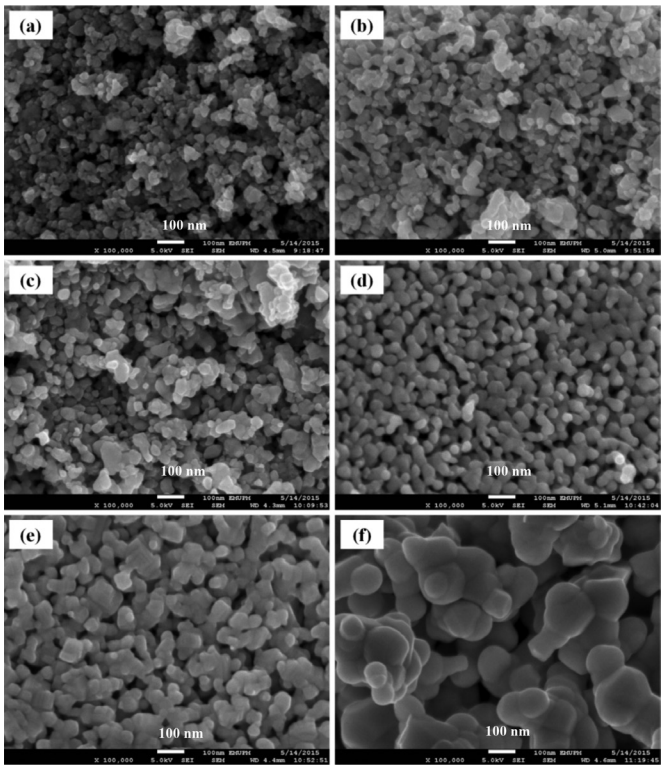

FIGURE 3. SEM micrographs of LSMO nanoparticles at calcination temperature of (a) 500, (b) 600, (c) 700, (d) 800, (e) 900 and (f) 1000ºC

TABLE 1. Average crystallite size, average particle size and magnetic properties of LSMO nanoparticles

Calcination temperature (ºC)	Average crystallite size (nm)	Average particle size (nm)	Saturation magnetization at 10G, Ms (emu/g)	Coercivity, Hc (G)	g- factor	ΔH_{pp} (mT)
500	18.6	~23	14.68	3.43	2.0118	400
600	21.1	~29	24.16	17.33	2.1566	420
700	21.9	~37	28.52	23.31	2.4556	436
800	30.2	~47	35.01	31.89	2.9862	443
900	32.1	~67	48.88	33.78	N.A.	-
1000	65.7	~163	53.37	23.53	N.A.	-

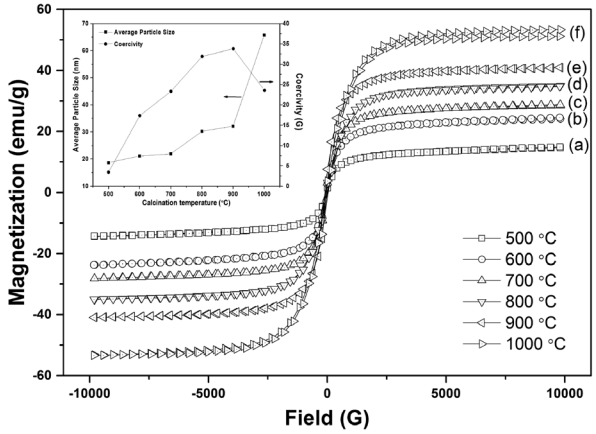

FIGURE 4. (a) Room temperature magnetization curves of LSMO nanoparticles calcination temperature of (a) 500, (b) 600, (c) 700, (d) 800, (e) 900, and (f) 1000ºC. inset Correlation between average particle size and coercivity of LSMO at various calcination temperatures (500-1000ºC)

(emu/g) with the increased of calcination temperature is clearly seen. This increment has proportional trend with the increasing of average particle size. As the average particle size increases, the magnetic disorder layers around the nanoparticles may be decreased and hence the ferromagnetic ordering increased which resulted in improving magnetization value (Shivakumara et al. 2007; Varma 2006). This behaviour was also observed in other magnetic nanoparticles synthesized using thermal treatment method such $BiFeO_3$ (Zahari et al. 2017).

Coercivity (H_c) is another essential magnetic behaviour that can be collected from ($M-H$) curve of LSMO nanoparticles. Coercivity value of each LSMO samples is shown in Table 1. The values of H_c are 3.43, 17.33, 23.31, 31.89, 33.78 and 23.53 G for samples calcined at 500, 600, 700, 800, 900, and 1000ºC, respectively. From Table 1 and inset of Figure 4 it is shown that the coercivity value increases when the *C.T.* increases from 500 to 900ºC, and then experienced a drop from at *C.T.* = 900 – 1000ºC. This phenomenon is due to the fact that the reduction of size of magnetic particle up to critical size is associated with the transformation from magnetic multi-domain to magnetic single domain and the increase of coercivity. As the size of magnetic particle further reduced the coercivity will decrease toward zero and the materials will exist superparamagnetic state (Papaefthymiou 2009). Therefore, the state of magnetic domains of LSMO nanoparticles, may be altered from single domain state in samples calcined at 500, 600, 700, 800, and 900ºC to multi domain state in with *C.T.* = 1000ºC. Sample calcined at 900ºC showed a maximum of coercivity value, hence the critical size of single domain state is supposed to be around the average particle size of ~67 nm.

Figure 5 shows the calcination temperature dependence of ESR spectra of LSMO nanoparticles measured at room temperature. The g-factor value of the samples was calculated using the following equation,

$$g = \frac{h\nu}{\beta H_r}$$

where g is g-factor; β is Bohr magneton ($9.2740 \times 10^{-24} JT^{-1}$); h is Planck's constant (6.621×10^{-34}); H_r is resonant magnetic field; and ν is microwave frequency. By increasing the calcination temperature, the g-factors value of the LSMO nanoparticle increased and different shape of ESR curves were observed. At 500°C calcination temperature, the ESR spectrum had wide and symmetric like shape. However, the ESR spectrum of this sample did not fit completely with Lorentz function (Figure 6), which indicates that the sample calcined at 500ºC may be dominated by paramagnetic phase beside small amount of ferromagnetic phase (Wu & Lin 2006). By increasing of the calcination temperature above 500°C, the symmetry of ESR curves degraded. The samples calcined at 600, 700, and 800ºC had almost the same shape but their peak to peak width, ΔH_{pp}, increased, (Table 1). In addition, the spectra shifted toward lower magnetic field with increasing calcination temperature. This indicates that the pronounced ferromagnetic phase that realized in sample calcined at 500ºC has been grown while paramagnetic phase reduces (Zhang et al. 2013). The symmetry of ESR curves degraded further for sample calcined at 900, 1000ºC. The symmetry degradation of ESR signal in previous samples and increase

of g-factor values, as shown in Table 1, suggests that the increase of calcination temperature will form stronger ferromagnetic phase and decrease of paramagnetic phase contamination at the surface of LSMO nanoparticles (Zhang et al. 2013). The coexistence of paramagnetic and ferromagnetic phases was also observed in LSMO nanoparticles prepared by sol-gel routes with three different gelation agents and calcined at 700°C at room temperature (below T_c) and in LSMO nanofibers prepared by electrospinning process (Wu & Lin 2006; Zhang et al. 2013).

The ESR spectra were measured for all nanoparticles above and below T_c of bulk LSMO, i.e. ≈ 370 K (100°C) system. Figure 6(a) and 6(b) shows the ESR spectra of samples calcined at 500 and 900ºC measured at temperature (T) 30, 50, 80, 110, 140, and 170°C. The ESR spectrum of sample calcined at 500ºC had symmetric, broadened peaks but is not completely fitted with Lorentz function at 30 and 50°C temperature. However, the peaks become narrower with higher symmetry and can be well fitted with Lorentz function at $T > 50$°C. This indicates that this sample is completely in the paramagnetic state at $T > 50$°C. On the other hand, the signal did not show symmetry curve at 30°C, 50°C and 80°C of samples calcined at 900°C due to the mixed phases of ferromagnetic and paramagnetic. As T increased to 110°C, the asymmetric behaviour is substituted by symmetrical signal indicating the paramagnetic phase has taken role in this region at this temperature. The signals are well-fitted with Lorentz function at 110, 140 and 170°C proving that the samples are in paramagnetic state at $T \geq 110$°C. This behaviour was also observed for samples calcined at 600, 700, 800 and 1000 where symmetrical spectra were observed at $T \geq 110$°C. Hence, from the results, one can estimate that the Curie temperature (T_c) of LSMO calcined at 500°C is in the range of 50°C (323 K) to 80°C (353 K) and it is in range of 80°C (353 K) to 110°C (383 K) for samples calcined at 600, 700, 800, 900, and 1000°C (Wu & Lin 2006). The estimated T_c of LSMO nanoparticles is in agreement with the phase diagram of LSMO (Fujishiro 1998).

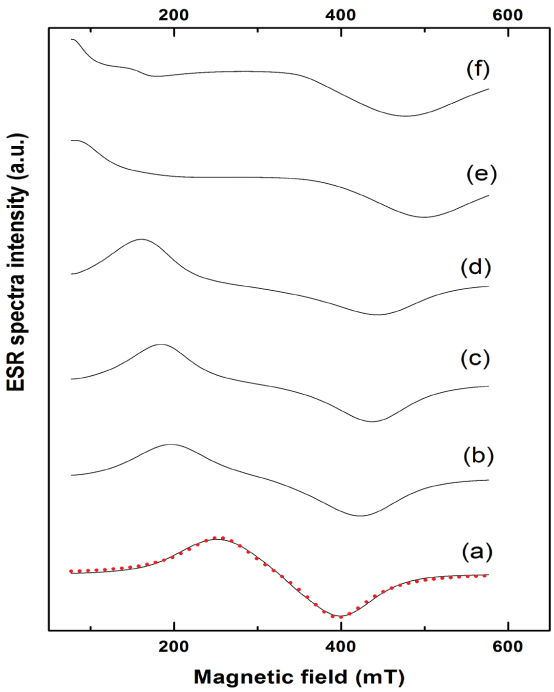

FIGURE 5. ESR spectra measured at room temperature of LSMO nanoparticles calcined (a) 500, (b) 600, (c) 700, (d) 800, (e) 900 and (f) 1000ºC., where red dot is Lorentz curve fit of ESR spectra for sample calcined at 500ºC

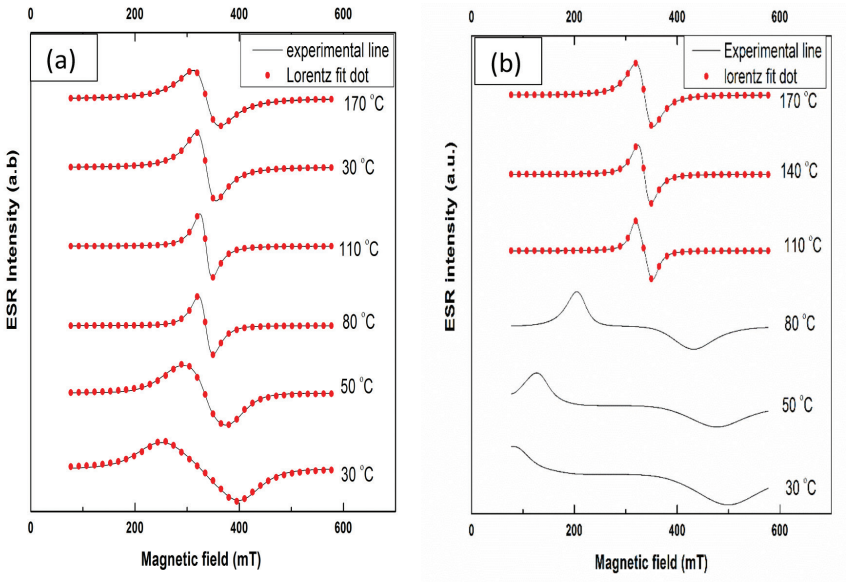

FIGURE 6. ESR spectra measured at temperature 30-170ºC for LSMO nanoparticles calcined at (a) 500ºC and (b) 900ºC. The red dot is Lorentz fitting of curves

CONCLUSION

The $La_{0.7}Sr_{0.3}MnO_3$ (LSMO) nanoparticles were successfully synthesized by thermal treatment of aqueous solution of metal nitrate and PVP that act as a capping agent. A single phase of LSMO was formed at calcination temperature calcination temperature (*C.T.)* ≥ 600°C. The average size of LSMO nanoparticles enlarged with increment of *C.T.* The H_c of LSMO samples increased from 3.43 G for LS500 to 33.78 G for sample calcined at 900°C and then decreased to 23.3 G for sample with *C.T.* of 1000°C due to the transition from single magnetic domain, i.e. at 67 nm for sample *C.T.* = 900, to magnetic multi-domain, i.e. at 163 nm for sample *C.T.* = 1000. The ESR spectrometer results were consentient with VSM results and indicated the coexistence of ferromagnetic and paramagnetic phases due to the disordered layers at the surface of LSMO nanoparticles that reduce with increasing calcination temperature. The T_c estimated from the ESR was agree with phase diagram of LSMO and it was in the range of 80 - 110°C for samples with *C.T.* above 600°C. Finally, this work demonstrates that thermal treatment, which is simple and environmentally friendly technique, can be used to prepare single phase nanoparticles of complex oxide, such as LSMO system.

ACKNOWLEDGMENTS

The authors would like to acknowledge the financial support from the Ministry of Education, Malaysia for the Fundamental Research Grant Scheme (FRGS 5524941).

REFERENCES

Andrade, V.M., Caraballo Vivas, R.J., Pedro, S.S., Tedesco, J.C.G., Rossi, A.L., Coelho, A.A., Rocco, D.L. & Reis, M.S. 2016. Magnetic and magnetocaloric properties of $La_{0.6}Ca_{0.4}MnO_3$ tunable by particle size and dimensionality. *Acta Materialia* 102: 49-55.

Daengsakul, S., Thomas, C., Siri, S., Thomas, I., Amornkitbamrung, V., Maensiri, S. & Mongkolkachit, C. 2009a. A simple thermal decoposition synthesis, magnetic properties and cytotoxicity of $La_{0.7}Sr_{0.3}MnO_3$ nanoparticles. *Applied Physics A: Materials Science & Processing* 96: 691-699.

Daengsakul, S., Thomas, I., Mongkolkachit, C., Siri, S., Amornkitbamrung, V., Maensiri, S. & Thomas, C. 2009. Magnetic and cytotoxicity properties of $La_{1-x}Sr_xMnO_3$ ($0<x<0.5$) nanoparticles prepared by a simple thermal hyro-decomposition. *Nanoscle Research Letter* 4: 839-845.

Drofenik, V. & Uskokovie, M. 2007. Four novel co-precipitation procedures for the synthesis of lanthanum strontium manganites. *Materials and Design* 28: 667-672.

Du, Y.K., Mou, Z.G., Hua, N.P., Jiang, L. & Yang, P. 2006. Thermal decomposition behaviors of PVP coated on platinum nanoparticles. *Journal of Applied Polymer Science* 99: 23-26.

Dutta, A., Gayathri, N. & Ranganathan, R. 2003. Effect of particle size on the magnetic and transport properties of $La_{0.875}Sr_{0.125}MnO_3$. *Physical Review B* 68: 54432-54438.

Dyakonov, V.A., Ślawska-Waniewska, N., Nedelko, E., Zubov, V., Mikhaylov, K., Piotrowski, A., SzytuŁ, S.B., Bazela, W., Kravchenko, Z., Aleshkevich, P., Pashchenko, A., Dyakonov, K., Varyukhin, V. & Szymczaka, H. 2010. Magnetic, resonance and transport properties of nanopowder of $La_{0.7}Sr_{0.3}MnO_3$ manganites. *Journal of Magnetism and Magnetic Materials* 322(20): 3072-3079.

Ehi-Eromosele, C.O., Ita, B.I., Iweala, E.E.J., Ogunniran, K.O., Adekoya, J.A. & Ehi-Eromosele, F.E. 2016. Structural and magnetic characterization of $La_{0.7}Sr_{0.3}MnO_3$ nanoparticles obtained by the citrate-gel combustion method: Effect of fuel to oxidizer ratio. *Ceramics International* 42(1, Part A): 636-643.

Fujishiro, H., Fukase, T. & Ikebe, M. 1998. Charge ordering and sound velocity anomaly in $La_xSr_{1-x}MnO_3$ ($x \geq 0.5$). *Journal of the Physical Society of Japan* 67: 2582-2585.

Ghosh, A., Gulnar, A.K., Suri, A.K. & Sahu, A.K. 2005. Synthesis and characterization of lanthanum strontium manganite. *Scripta Materialia* 52: 1305-1309.

Gupta, A. & Sun, J.Z. 1999. Spin-polarized transport and magnetoresistance in magnetic oxides. *Journal of Magnetism and Magnetic Materials* 200(1-3): 24-43.

Hwang, H.Y., Cheong, S.W., Ong, N.P. & Batlogg, B. 1996. Spin-polarized intergrain tunneling in $La_{2/3}Sr_{1/3}MnO_3$. *Physical Review Letters* 77(10): 2041-2044.

Karthikeyan, S. & Ravi, A. 2014. Effect of calcination temperature on $La_{0.7}Sr_{0.3}MnO_3$ nanoparticles synthesized with modified sol-gel route. *Physics Procedia* 54: 45-54.

Lee, S.M., Chon, G.B., Lee, C.G., Koo, B.H. & Lim, H.S. 2006. Hydrothermal reaction for the preparation of $La_{0.7}Ca_{0.3}MnO_3$ and $La_{0.7}Sr_{0.3}MnO_3$. *Journal of the Korean Physical Society* 48: 1409-1412.

Lopez-Quintela, M.A., Rivas, J., Rivadulla, F. & Hueso, L.E. 2003. Intergranular magnetoresistance in nanomanganites. *Nanotechnology* 14: 212-219.

Millis, A.J., Littlewood, P.B. & Shramin, B.I. 1995. Double exchange alone does not explain the resistivity of $La_{2/3}Sr_{1/3}MnO_3$. *Physical Review Letters* 74: 5144-5147.

Moradi, J., Ghazi, M.E., Ehsani, M.H. & Kameli, P. 2014. Structural and magnetic characterization of $La_{0.8}Sr_{0.2}MnO_3$ nanoparticles prepared via a facile microwave-assisted method. *Journal of Solid State Chemistry* 215: 1-7.

Naseri, M.G., Elias, B.S., Mansor, H., Abdul Halim, S. & Hossein Abasstabar, A. 2011a. Synthesis and characterization of zinc ferrite nanoparticles by a thermal treatment method. *Solid State Communications* 151(14-15): 1031-1035.

Naseri, M.G., Elias B.S., Hossein Abbastabar, A., Mansor, H. & Abdul Halim, S. 2011b. Simple preparation and characterization of nickel ferrite nanocrystals by a thermal treatment method. *Powder Technology* 212(1): 80-88.

Pan, K.Y., Lim, K.P., Daud, W.M., Chen, S.K. & Halim, S.A. 2012. Effect of sintering temperature on microstructure, electrical and magnetic properties of $La_{0.85}K_{0.15}MnO_3$ prepared by sol-gel method. *Journal of Superconductivity and Novel Magnetism* 25: 1177-1183.

Papaefthymiou, G.C. 2009. Nanoparticle magnetism. *Nano Today* 4(5): 438-447.

Rajagopal, R., Mona, J., Kale, S.N., Bala, T., Pasricha, R., Poddar, P., Sastry, M., Prasad, B.L.V., Kundaliya, D.C. & Ogale, S.B. 2006. $La_{0.7}Sr_{0.3}MnO_3$ nanoparticles coated with fatty amine. *Applied Physics Letters* 89(2): 23107.

Shivakumara, C., Prakash, A.S., Vasanthacharya, N.Y. & Belakki, M.B. 2007. Rapid synthesis of ferromagnetic $La_{1-x}Na_xMnO_3$ ($0.00 \leq x \leq 0.25$) by the Solution Combustion Method. *Journal of the American Ceramic Society* 90: 3852-3858.

Teng, F. 2009. Hydrothermal synthesis and their catalytic properties of manganites nanowires. *Solid State Sciences* 11: 1643-1648.

Thorat, N.D., Pawar, S.H., Barick, K.C., Betty, C.A., Ningthoujam, R.S. & Shinde, K.P. 2012. Polyvinyl alcohol: An efficient fuel for synthesis of superparamagnetic LSMO nanoparticles for biomedical apllication. *Dalton Transactions* 41: 3060-3071.

Urushibara, A., Arima, T., Asamitsu, A., Kido, G., Tokura, Y. & Moritomo, Y. 1995. Insulator-metal transition and giant magnetoresistance in $La_{1-X}Sr_xMnO_3$. *Physical Review B* 51: 14103-14109.

Varma, A. & Gaur, G.D. 2006. Sintering temperature effect on electrical transports and magnetoresistance of nanophasic $La_{0.7}Sr_{0.3}MnO_3$. *Journal of Physics: Condensed Matter* 18: 8837-8846.

Wu, J.H. & Lin, J.G. 2006. Study on the phase separation of $La_{0.7}Sr_{0.3}MnO_3$ nanoparticles by electron magnetic resonance. *Journal of Magnetism and Magnetic Materials* 304(1): e7-e9.

Zahari, R.M., Shaari, A.H., Abbas, Z., Baqiah, H., Chen, S.K., Lim, K.P. & Kechik, M.M.A. 2017. Simple preparation and characterization of bismuth ferrites nanoparticles by thermal treatment method. *Journal of Materials Science: Materials in Electronics* 28(23): 17932-17938.

Zener, C. 1951. Interaction between the *d*-Shell in the transition metals. II. Ferromagnetic compounds of manganese with perovskite structure. *Physical Review* 82: 403.

Zhang, Y., Weiwei, P., Dong, J., Wang, Z., Liu, Q. & Wang, J. 2013. Morphology dependence of electron spin resonance investigation on structure controllable hollow $La_{0.7}Sr_{0.3}MnO_3$ nanofibres. *Journal of Physics D: Applied Physics* 46(10): 105001.

Department of Physics
Universiti Putra Malaysia
43400 UPM Serdang, Selangor Darul Ehsan
Malaysia

*Corresponding author; email: ahalim@upm.edu.my

Received: 16 July 2018
Accepted: 20 September 2018